KeAi
CHINESE ROOTS
GLOBAL IMPACT

#### Contents lists available at ScienceDirect

# Petroleum Science

journal homepage: www.keaipublishing.com/en/journals/petroleum-science



# Original Paper

# Enhanced recovery in heavy oil reservoirs with interlayers using flue gas-assisted VH-SAGD: A 2D visualization study



Bin-Fei Li <sup>a,b,\*</sup>, Bo-Liang Li <sup>a,b</sup>, Xin-Ge Sun <sup>c</sup>, Di Zhu <sup>a,b</sup>, Sen Chen <sup>c</sup>, Zhao-Min Li <sup>a,b</sup>, Lei Tao <sup>d</sup>, Jun-Hao Zhang <sup>a,b</sup>

- <sup>a</sup> School of Petroleum Engineering, China University of Petroleum (East China), Qingdao, 266580, Shandong, PR China
- b Key Laboratory of Unconventional Oil & Gas Development (China University of Petroleum (East China)), Ministry of Education, Qingdao, 266580, Shandong, PR China
- <sup>c</sup> Xinjiang Oilfield Company, PetroChina, Karamay, 834000, Xinjiang, PR China
- <sup>d</sup> School of Petroleum Engineering, Changzhou University, Changzhou, 213164, Jiangsu, PR China

#### ARTICLE INFO

#### Article history: Received 21 October 2024 Received in revised form 7 May 2025 Accepted 9 May 2025 Available online 11 May 2025

Edited by Yan-Hua Sun

Keywords: VH-SAGD Flue gas Interlayer Steam Carbon emissions Enhanced oil recovery

# ABSTRACT

The potential of the vertical-horizontal well hybrid SAGD technique for developing shallow heavy oil reservoirs is gradually being realized. However, challenges remain in terms of low thermal efficiency and high carbon emissions in reservoirs with interlayers. Currently, there is limited research on the lowcarbon strategy of coupling exhaust gas from steam boilers with the VH-SAGD technique. Herein, considering heterogeneity, a series of flue gas-assisted VH-SAGD experiments were conducted employing a high-performance 2D visualization model. The mechanism of enhanced recovery of flue gas in VH-SAGD and the effect of its injection methods were studied, with a focus on steam chamber development and oil saturation distribution. Crucially, the interlayer length was optimized to enhance oil recovery, providing a new perspective for well location design in heavy oil reservoirs with interlayers. The results showed that flue gas, as an additive, could fully exploit the well-type advantage of VH-SAGD. By supplementing energy at the reservoir top, flue gas effectively promoted steam chamber development, expanded the oil drainage area of VH-SAGD, and increased the oil recovery from 58.9% to 71.7%. The flow channels formed by pre-injection flue gas accelerated the early-stage expansion of the steam chamber while also inducing lateral migration of steam, slowing steam rise, and consequently increasing the heating range within the low-permeability layer. When the distance between the vertical and horizontal wells was set to twice the interlayer length, the negative effects of the interlayer were more effectively turned into advantages. Because when the lateral development distance of the steam chamber in the low-permeability layer slightly exceeds the interlayer, enhanced heating of the lower part of the reservoir occurred through vertical convection of rising steam and returning condensate. The research results contribute to reducing carbon emissions from steam-based heavy oil extraction while advancing the maturity of VH-SAGD.

© 2025 The Authors. Publishing services by Elsevier B.V. on behalf of KeAi Communications Co. Ltd. This is an open access article under the CC BY-NC-ND license (http://creativecommons.org/licenses/by-nc-nd/4.0/).

## 1. Introduction

Global conventional petroleum reserves, prized for their extractability, are declining steadily. This has positioned heavy oil and extra-heavy oil—characterized by higher pour points and viscosities and limited fluidity—as critical development targets (Santos et al., 2014). Statistical data from the American Association

development. However, heavy oil extraction remains technologically challenging due to its high asphaltene content and the presence of sulfur, oxygen, nitrogen, and other heteroatoms, which substantially increase production costs (Speight, 2013). Recently,

of Petroleum Geologists (AAPG) indicate that untapped heavy oil amounts to  $9380 \times 10^8$  tons, accounting for nearly 70% of total petroleum reserves (Guo et al., 2016; Bata et al., 2019; Li et al.,

2020). These findings provide critical guidance for nations to

navigate global uncertainties and transition toward sustainable

enhancing the efficiency and economic viability of heavy oil

E-mail address: libinfei999@126.com (B.-F. Li).

<sup>\*</sup> Corresponding author.

development has emerged as a priority research area in the oil and gas industry, aiming to strengthen its market competitiveness.

The primary challenge in heavy oil extraction lies in achieving significant viscosity reduction (Pierre et al., 2004). Unlike conventional crude oil, heavy oil exhibits limited fluidity under reservoir conditions and cannot be directly pumped out of the ground. However, its viscosity is highly temperature-sensitive, decreasing by up to 50% with a temperature increase of 8–10 °C (Bai, 2015). Thus, injecting high-enthalpy steam into formations has become the predominant commercial recovery method, including cyclic steam stimulation (CSS), steam flooding, steamassisted gravity drainage (SAGD), and in-situ combustion (Mai et al., 2009; Zhao et al., 2014; Wei et al., 2022). Among these, the SAGD proposed by Butler et al. (1981) has proven particularly effective for extra-heavy oil development. However, because the dual-horizontal well configuration provides only vertical drive, traditional SAGD is highly effective in medium-thick layered and thick massive extra-heavy oil reservoirs (Al-Bahlani and Babadagli, 2009). Its applicability is limited in heavy oil reservoirs with thicknesses of less than 20 m or those with developed interlayers (Nguyen et al., 2012; Huang et al., 2016; Cui et al., 2022). Additionally, as shale-rich interlayers gradually become longer and approach the injection well, the constraints on reservoir steam chamber expansion become more pronounced (Huang et al., 2019; Kumar and Hassanzadeh, 2021).

The vertical-horizontal well hybrid SAGD (VH-SAGD) is an improved version of the traditional SAGD technology, utilizing a combination of vertical and horizontal wells to improve steam chamber expansion efficiency. Compared to traditional SAGD, VH-SAGD offers better control over steam injection and fluid flow paths, thereby increasing the oil recovery (Sasaki et al., 2001; Wang et al., 2023b). Tamer and Gates (2012) evaluated the effect of the geometric configuration of steam injection wells on oil drainage using a 3D reservoir model that incorporated geological parameters. They found that multiple vertical wells delivered steam to the formation more efficiently than a single horizontal well. Tao et al. (2021) optimized well spacing through laboratory experiments, suggesting that for a thick, approximately 15-m ultraheavy oil reservoir, spacing wells between 15 and 20 m could improve VH-SAGD performance. The primary advantage of VH-SAGD is the integration of horizontal dynamic forces into SAGD, creating a dual mechanism of displacement and oil drainage. Additionally, overcoming the longitudinal shielding effect of the interlayer can enhance production efficiency in heavy oil reservoirs with thinner oil layers (Zhao et al., 2023; Gao et al., 2022; Hocking et al., 2011). However, like other steam-based recovery methods, challenges such as low thermal efficiency, and high carbon emissions must be optimized and addressed.

Steam generation involves the combustion of coal or natural gas, releasing CO<sub>2</sub>-laden flue gas into the atmosphere, exacerbating the greenhouse effect and contradicting the current emphasis on low-carbon development. To improving steam thermal utilization efficiency, various additives such as chemicals, non-condensable gases (NCG), solvents, and nanoparticles have been considered for use alongside steam in heavy oil development (Xi et al., 2019; Nasr and Ayodele, 2006; Alomair and Alajmi, 2022; Lu et al., 2024), and some strategies have shown significant effects. For instance, NCG can lower the saturation temperature, which may slightly hinder bitumen mobilization; however, it generally increases the oil/steam ratio (Austin-Adigio and Gates, 2019; Lu et al., 2024; Jamshid-nezhad, 2022). Furthermore, the injected NCG forms a thermal insulating layer that effectively reduces heat loss, and under optimized well configurations, it has demonstrated significant improvements in SAGD performance (Zhang and Maini, 2020; Liu et al., 2012). These findings not only provide a theoretical

foundation for SAGD optimization but also emphasize critical parameters for improving heat transfer and flow characteristics (Huang et al., 2015). Considering cost-effectiveness, material availability, and environmental impact, flue gas demonstrates superior practical potential among the available NCG options. The relatively low compressibility of N<sub>2</sub> in flue gas, combined with its role in formation energy supplementation during steam channeling, helps maintain pressure stability and enhances oil production rates (Gao et al., 2008; Chen et al., 2020). Additionally, the mechanism underlying enhanced thermal recovery by flue gas involves its impact on heavy oil properties. Based on laboratory PVT experiments and theoretical calculations, Wang et al. (2017) and Li et al. (2024) observed that the viscosity of heavy oil decreases significantly upon flue gas dissolution, with the reduction degree positively correlated to the gas solubility. Furthermore, our recent findings indicated that flue gas promotes resin hydrocracking and allosterism in heavy oil, improving steam distillation efficiency (Li et al., 2023).

Traditional SAGD research has extensively explored factors such as gas injection methods and well placement. However, studies combining flue gas with VH-SAGD are relatively rare, and the potential impacts of this combination warrant further investigation. In this work, considering heterogeneity, a series of experiments combining flue gas with VH-SAGD were conducted using a high-temperature-resistant 2D visualization model. The enhancement mechanisms of flue gas in VH-SAGD and the impact of its injection method were studied from various perspectives, such as steam chamber development and production dynamics. The length of the interlayer was also optimized to improve recovery efficiency. This novel approach aims to efficiently utilize typically wasted flue gas resources, simultaneously reducing carbon emissions and advancing the maturity of VH-SAGD technology.

## 2. Experimental section

#### 2.1. Materials

The two types of crude oil in this work were sourced from two distinct heavy oil blocks in the Xinjiang Oilfield, China, with heavy fraction (resin + asphaltene) contents of 25.26 and 30.99 wt%, respectively. The viscosities of these oils at 30 °C and 0.1 MPa were  $6.3 \times 10^4$  and  $1.24 \times 10^5$  mPa·s, respectively, which are classified as extra-heavy oils by the International Standardization Organization (ISO), and detailed parameter information is provided in Table 1. To ensure that the results and discussion were more realistic, the oil samples were diluted with diesel fuel based on similarity criteria (SY/T 7068-2016) and experimental model parameters, and viscosity-temperature curves of the diluted simulated oil samples are shown in Fig. 1. The gas used was flue gas, which was prepared with N<sub>2</sub> and CO<sub>2</sub> at a molar ratio of 4:1. The purity of both N<sub>2</sub> and CO<sub>2</sub> was 99.9%, as determined by the Qingdao Tianyuan Gas Manufacturing Company. The steam used was prepared from ultrapure water by boiling, and the simulated formation water used comprised ultrapure water, 800 mg·L<sup>-1</sup> CaCl<sub>2</sub> and 35000 mg·L<sup>-1</sup> NaCl, with a resistivity of 18.2 M $\Omega$ ·cm.

# 2.2. Apparatus

The 2D oil displacement device consisted of four main components, namely, a fluid injection system, an oil displacement model, a data acquisition system, and a fluid collection system, as shown in Fig. 2. In the fluid injection system, two ISCO piston pumps (model 100DX, Teledyne Co., Ltd., USA; pressure range: 0–50 MPa; flow rate range: 0–50 mL·min $^{-1}$ ; accuracy:  $\pm 0.001$  mL·min $^{-1}$ ) were utilized

 Table 1

 Parameters of the crude oils used in the experiment.

Oil sample No.	Measurement conditions		Viscosity, mPa·s	Density, kg⋅m <sup>-3</sup>	Mass fraction, wt%			
	Temperature, °C	Pressure, atm			Saturates	Aromatics	Resins	Asphaltenes
1	30	1	$6.30 \times 10^{4}$	943	42.94	31.80	22.70	2.56
2	30	1	$1.24\times10^{5}$	948	32.87	36.14	25.10	5.89

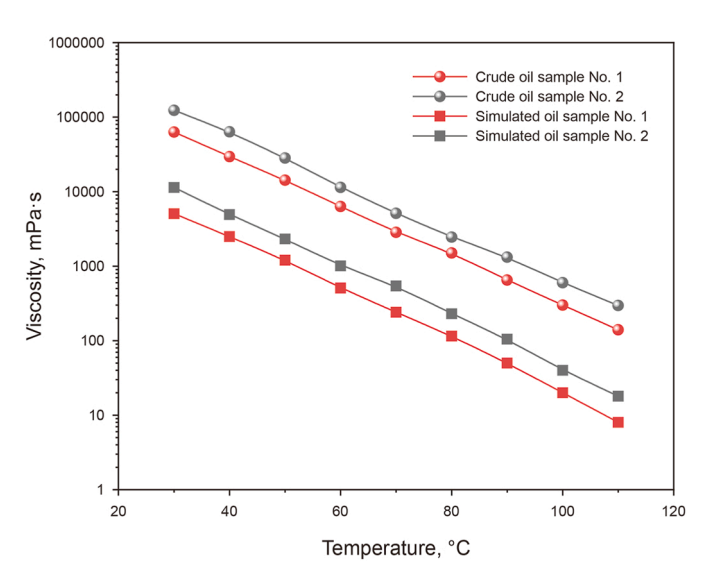


Fig. 1. Viscosity-temperature curves of the oil samples.

to provide the driving force for the flow of steam, formation water, and ultraheavy oil. Prior to injection into the model, steam was directly produced by a steam generator (model GL-1; Huaan Scientific Instrument Co., Ltd., China; temperature range: 0–350  $^{\circ}\text{C}$ ; pressure range: 0–25 MPa). To accurately control the injection of flue gas, a mass-flow gas meter (model Sla58550, Brooks, USA; flow rate range: 0–30 mL·min $^{-1}$ ) was connected between the flue gas cylinder and oil displacement model.

The oil displacement model included a 2D visualization

apparatus (model LW-5060; Haian Petroleum Research Instrument Co., Ltd., China; pressure range: 0-30 MPa; temperature range: 0-300 °C) and a matching heating controller (Fig. 3). The visual area of the apparatus was 50 cm in length and 40 cm in width. The visualization window was made of high-temperature and high-pressure resistant borosilicate glass with a thickness of 7 cm. To ensure airtightness of the model and further enhance the pressure resistance of the window, a superheavy steel plate with a  $4 \times 3$  well-shaped grids was pressed onto the glass (Fig. 3(a)). Nut holes were placed on the side of the model to facilitate the arrangement of the wells (Fig. 3(b)). Eight modular tracking heating panels were staggered on the back of the model (Fig. 3(c)) to provide continuous heating of the target area. Simultaneously, there were 60 uniformly distributed temperature probes interconnected inside the model for real-time monitoring of temperature field changes. The compaction degree of the sand layer could be controlled by a removable piston surrounding the temperature probes. The data acquisition system included a computer and a high-definition camera (Sony ZV-E10) for collecting images, temperature values, and pressure data during the experiments. The liquid collection system included a back-pressure valve and a graduated cylinder to control the model pressure and to record the oil and water production dynamics during displacement.

# 2.3. Model parameter calculation

The experimental model was designed using similarity criteria to maintain proportionality with actual reservoir conditions. The obtained model parameters are listed in Table 1. The detailed transformation procedure of the parameters is as follows:

First, the similarity criterion R was employed to connect the

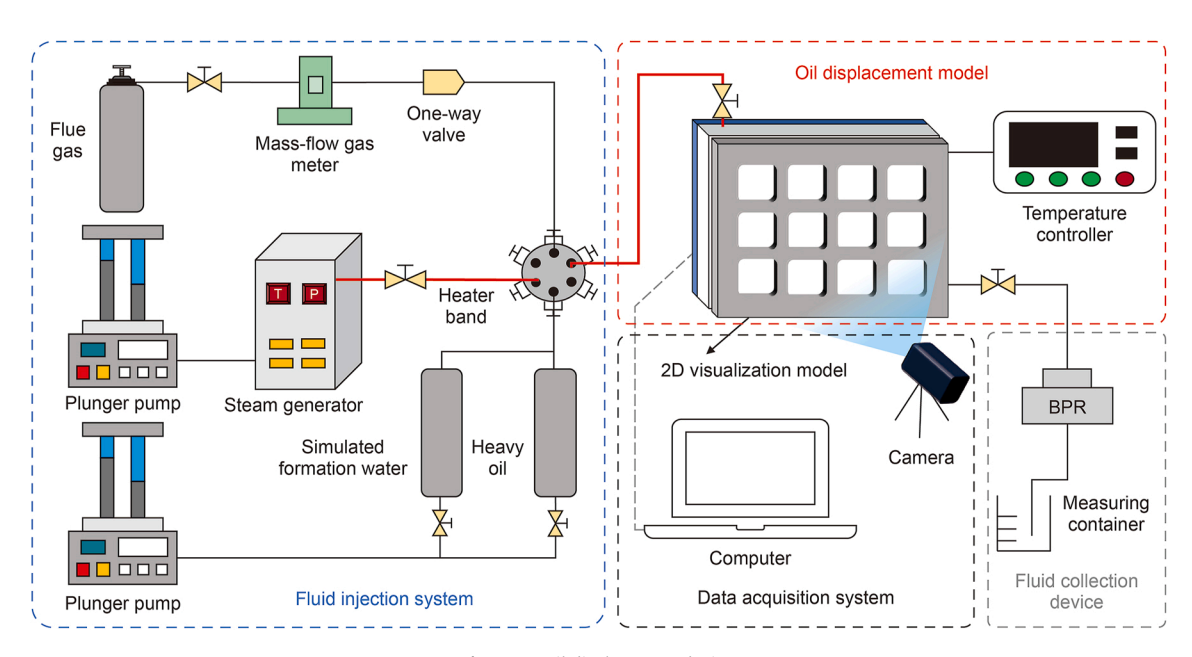
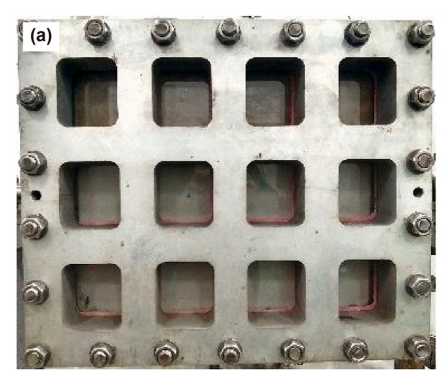


Fig. 2. 2D oil displacement device.





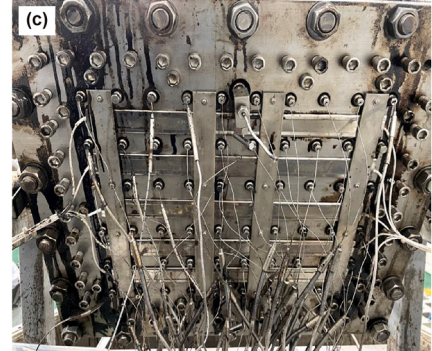


Fig. 3. Two-dimensional visualization model. (a) Front of the model; (b) side of the model; (c) back of the model.

model with the geometric dimensions of the reservoir, with the main physical parameters of the well spacing and reservoir size, as expressed in Eq. (1). The profile depth of the model was 1.2 cm.

$$R = \frac{L_{\rm m}}{L_{\rm f}} \tag{1}$$

Subsequently, to simulate the production time in the experimental process, Eq. (2) from the array of similarity criteria was introduced.

$$\frac{t_{\rm m}}{t_{\rm f}} = R^2 \cdot \frac{\alpha_{\rm of}}{\alpha_{\rm om}} \tag{2}$$

The conversion of steam injection rate from the actual reservoir to the physical simulation was achieved by Eq. (3). The perforation length  $\omega$  of the horizontal well in the actual reservoir was 300 m.

$$\frac{q_{\rm m}}{q_{\rm c}} = R \cdot \frac{\alpha_{\rm om} \phi_{\rm m}}{q_{\rm c} c \phi_{\rm c}} \tag{3}$$

The model permeability was calculated by combining dimensionless flow functions, as shown in Eq. (4):

$$\frac{\left(\frac{K}{\mu_{o}}\right)_{m}}{\left(\frac{K}{\mu_{o}}\right)_{f}} = \frac{1}{R} \frac{\alpha_{om} \Delta \rho_{f}}{\alpha_{of} \Delta \rho_{m}}$$
(4)

Finally, the initial pressure and initial temperature of the model were determined by Eqs. (5) and (6), respectively.

$$\overline{p} = \frac{p - p_{\min}}{p_{\max} - p_{\min}} \tag{5}$$

$$\overline{T} = \frac{T - T_{\min}}{T_{\max} - T_{\min}} \tag{6}$$

where  $L_{\rm m}$  is the well spacing between the injection and production wells in the model, m;  $L_{\rm f}$  is the well spacing between the injection and production wells on site, m; R is the similarity ratio, dimensionless;  $t_{\rm m}$  is the experimental production time, years;  $t_{\rm f}$  is the on-site production time, years;  $q_{\rm m}$  is the simulated steam injection rate,  ${\rm m}^3 \cdot {\rm d}^{-1}$ ;  $q_{\rm f}$  is the on-site steam injection rate,  ${\rm m}^3 \cdot {\rm d}^{-1}$ ;  $\alpha_{\rm of}$  is the thermal diffusion rate of heavy oil on site,  ${\rm m}^2 \cdot {\rm s}^{-1}$ ;  $\alpha_{\rm om}$  is the simulated oil thermal diffusion rate,  ${\rm m}^2 \cdot {\rm s}^{-1}$ ;  $\phi_{\rm m}$  is the porosity of the reservoir;  $\phi_{\rm f}$  is the model porosity; K is the permeability, mD;  $\mu_{\rm o}$  is the viscosity of crude oil at the temperature of the steam chamber edge, mPa·s;  $\overline{p}$  is the average pressure, MPa;  $p_{\rm min}$  is the minimum pressure, MPa;  $p_{\rm max}$  is the maximum pressure, MPa;  $\overline{T}$  is the average temperature, °C;  $T_{\rm min}$  is the minimum temperature,

 $^{\circ}$ C; and  $T_{\text{max}}$  is the maximum temperature,  $^{\circ}$ C.

# 2.4. Experimental procedures

# 2.4.1. Two-dimensional VH-SAGD experiment

The wells were arranged based on the model parameters calculated in Section 2.3. The injection well (vertical well) was positioned 2 cm from the left side of the model. The production well was located 2 cm above the bottom of the model, horizontally aligned with the tail end of the injection well at 35 cm. A clay interlayer with a permeability from  $5.1 \times 10^{-6}$  to  $6.0 \times 10^{-6}$   $\mu m^2$  was established in the middle of the model, measuring 2 cm in thickness and 15 cm in length. Additionally, a caprock made of the same material as the interlayer was placed at the top of the model to maintain the thickness of the reservoir at 20 cm. The layout is shown in Fig. 4.

It is vital to note that the heavy oil reservoir simulated in this work is a reverse stratum formation, with an average permeability of  $7600\times10^{-3}~\mu\text{m}^2$  required for the model. The permeability ratio between the high-permeability and low-permeability zones is 2 (Table 2). Therefore, when establishing the clay interlayer, 80-mesh and 120-mesh quartz sands were used to fill the high-permeability and low-permeability zones, with permeabilities of  $10000\times10^{-3}$  and  $5000\times10^{-3}~\mu\text{m}^2$ , respectively. Tempered glass and steel plates were positioned on the rubber sealing ring at the model edges, and the detachable bolts on the back of the model were tightened. After 12 h of vacuum pumping, the vertically placed model was sequentially saturated with water and crude oil at a rate of 1 mL·min $^{-1}$ , with the back-pressure regulator (BPR) set to 1 MPa. Subsequently, the model was heated to 100 °C and maintained for 24 h.

Before the experiment begins, the pipeline connecting the steam generator and the model needs to be preheated to 100 °C with a heating belt to prevent steam liquefaction. The injection

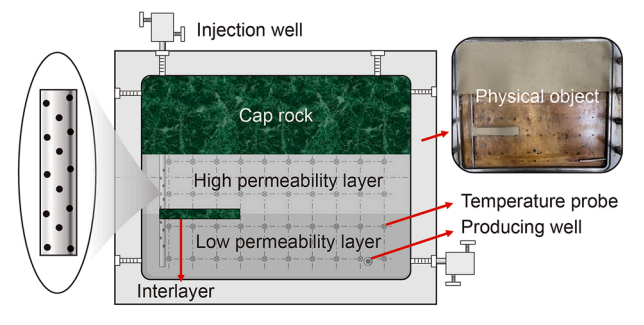


Fig. 4. Well location arrangement for VH-SAGD.

**Table 2** Matching parameters of the reservoir and the model.

Physical property	Field parameter	Model parameter
Geometrical dimensions, m	50 × 20	0.5 × 0.2
Injection-production well spacing, m	35	0.35
Porosity, %	27	38
Average permeability, 10 <sup>-3</sup> μm <sup>2</sup>	1200 (800/1600)	7600 (5000/10000)
Oil saturation, %	66	90
Oil viscosity @100 °C, mPa·s	300	20
Thermal diffusivity of crude oil, m <sup>2</sup> ·s <sup>-1</sup>	$8 \times 10^{-8}$	$7.6 \times 10^{-8}$
Production time, years	6.5	$6.8 \times 10^{-4}$ (i.e. 6 h)
Perforation length of the horizontal well, m	1.2	0.12
Steam injection rate, m <sup>3</sup> ·d <sup>-1</sup>	$0.64 (150 \text{ t} \cdot \text{d}^{-1})$	$8.64 \times 10^{-3} (6 \text{ mL} \cdot \text{min}^{-1})$
Original pressure, MPa	1.1 (average value)	1
Original temperature, °C	100 (average value)	100
R	0.01	0.01

parameters of steam and flue gas are listed in Table 3. Notably, in the three groups of flue gas-assisted VH-SAGD experiments, flue gas injection was stopped once the total injected volume reached 5.0 PV. During the process, a high-definition camera was used to capture the development characteristics of the steam chamber. The experiment was stopped when the water cut in the produced liquid exceeded 98%.

# 2.4.2. Determination of the oil saturation in oil sands

To analyze the impact of displacement methods on the extent of residual oil recovery, oil sand samples were collected from the model for oil content determination (Zhang et al., 2014). First, a measured quantity of oil sand ( $m_1$ ) was wrapped in filter paper and placed in a constant-pressure dropping funnel. Then, a certain volume of solvent was added to a round-bottom flask containing

**Table 3** Experimental parameters.

Displacement mode	Simulated oil sample No.	Injection method of gas	Porosity, %	Permeability, 10 <sup>-3</sup> μm <sup>2</sup>	Gas injection rate, mL·min <sup>-1</sup>	Steam injection rate, mL·min <sup>-1</sup>
VH-SAGD	1	1	38.10	5147/9948	0	6
Flue gas-assisted VH-	1	Co-injection	39.17	5030/9761	6	6
SAGD	2	Co-injection	39.38	5152/9647	6	6
	1	Gas pre-injection	38.84	5103/9832	6	6

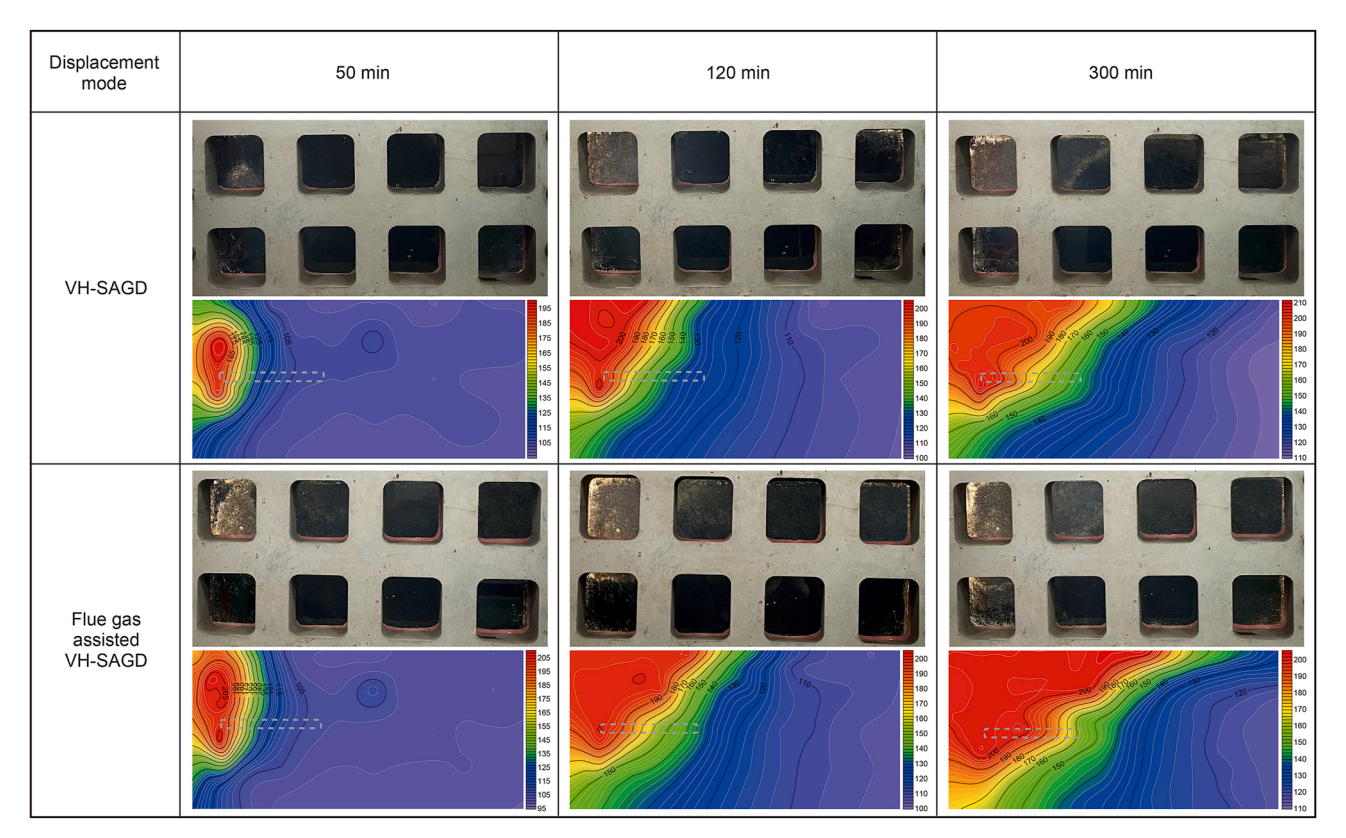


Fig. 5. Steam chamber expansion and temperature field changes in VH-SAGD and flue gas-assisted VH-SAGD.

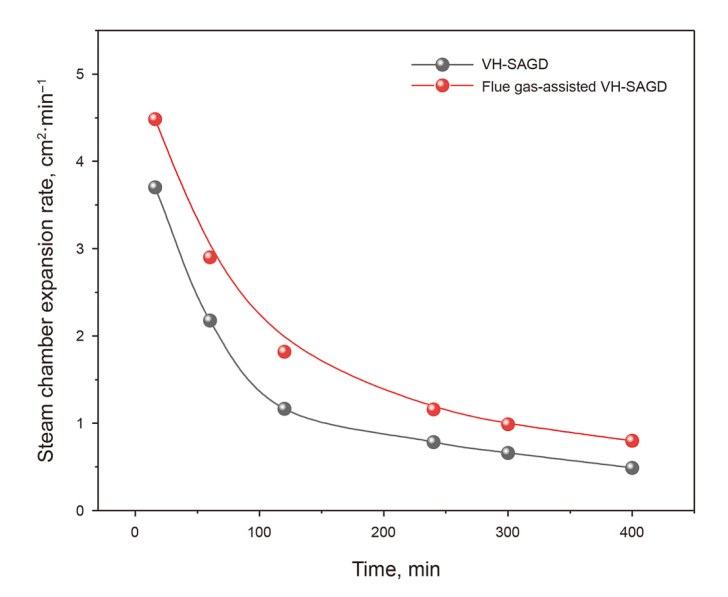


Fig. 6. Comparison of steam chamber expansion rate.

zeolite. The flask was connected to the funnel, and the solvent was heated to evaporate into the funnel, where it extracted heavy oil from the oil sand. Once enough volume of solvent accumulated, the mixture was refluxed into the flask. Heating ceased when the refluxed solvent in the funnel became colorless. The sample in the funnel was then dried in an oven at a controlled temperature for 4 h and weighed to determine the mass of quartz sand  $(m_2)$ . Subsequently, the extracted liquid in the flask was distilled until no solvent remained. The residual viscous liquid was dried for an additional 3 h, and its mass  $(m_3)$  was determined by subtracting the flask's mass, representing the heavy oil content in the oil sand.

Due to the destruction of the porous structure of the oil sand during extraction, direct measurement of oil saturation at the sampling location was unfeasible. Instead, oil saturation was calculated based on the determined oil content in the oil sand, as follows:

$$S_{\rm o} = \frac{V_{\rm o}}{V_{\rm p}} \times 100\% \tag{7}$$

$$V_0 = \frac{m_3}{\rho_0} \tag{8}$$

$$V_{\rm p} = \frac{m_2}{\rho_{\rm sand}} \times \frac{\phi}{1 - \phi} \tag{9}$$

where  $S_0$  is the oil saturation;  $V_0$  is the volume of crude oil extracted from the oil sand, mL;  $V_p$  is the pore volume of the porous medium (before saturation with crude oil), mL;  $m_2$  is the mass of quartz sand in the oil sand, g;  $m_3$  is the mass of crude oil in the oil sand, g;  $\rho_0$  is the density of crude oil in the oil sand, g·cm<sup>-3</sup>; and  $\rho_{sand}$  is the density of quartz sand in the oil sand, g·cm<sup>-3</sup>.

# 3. Results and discussion

#### 3.1. Effect of flue gas on VH-SAGD

To investigate the oil recovery characteristics of VH-SAGD in reservoirs with an interlayer and the influence of flue gas on this process, 2D visualization experiments were conducted with simulated oil sample No. 1, including VH-SAGD and flue gas-assisted VH-SAGD. The analysis focused on the steam chamber development characteristics, oil displacement dynamics, and distribution of the residual oil saturation in reservoirs with interlayers.

# 3.1.1. Steam chamber development

The quality of steam chamber development is pivotal in enhancing the recovery of heavy oil through steam-based extraction methods (Liu et al., 2018; Pang et al., 2021). Fig. 5 shows the steam chambers and corresponding temperature fields at different times in the VH-SAGD and flue gas-assisted VH-SAGD experiments. At the same moment, the shapes of the steam-affected area and temperature field closely match, which indicates that the experimental results are accurate and reliable.

Due to the large lateral distance between the vertical and horizontal wells, a brief piston displacement process occurs during

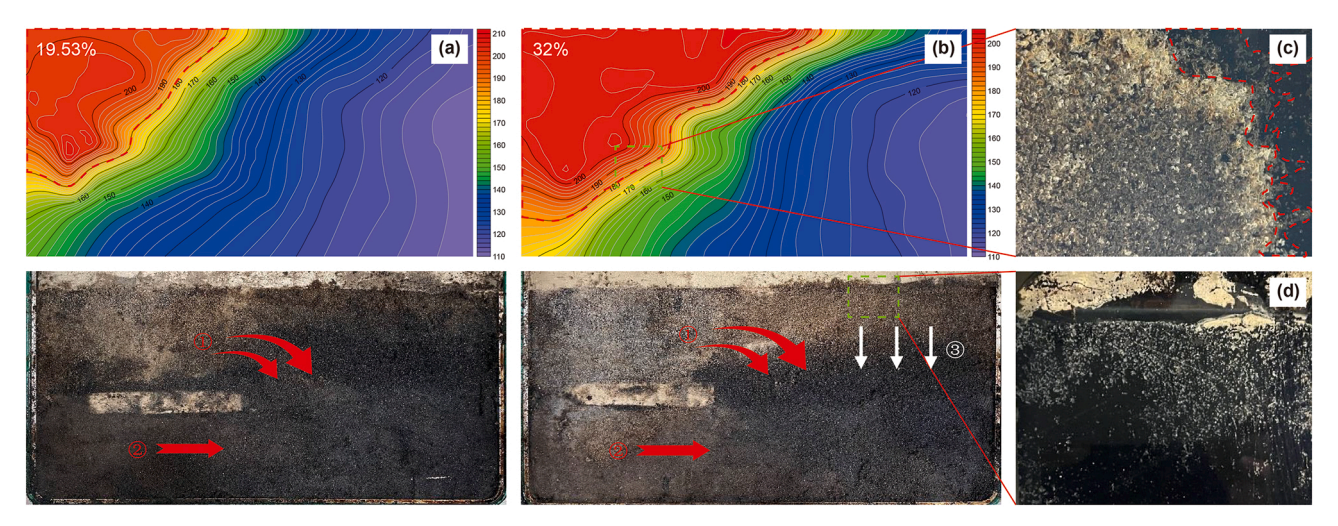


Fig. 7. Oil sand distribution and typical displacement phenomena. (a) Steam chamber and fluid flow at the end of VH-SAGD; (b) steam chamber and fluid flow at the end of flue gas-assisted VH-SAGD; (c) fingering effect of gas; (d) oil drainage at the top of the model.

the early development stage. When the oil saturation around the vertical well decreases, steam gradually occupies oil containing pores, forming the steam chamber. In the first 50 min of VH-SAGD, the steam chamber primarily develops in the perforation segment of the vertical well, with slightly better development in the upper part of the interlayer. During the middle stage of development (50–120 min), once the steam chamber reaches the cap rock, it

begins to expand laterally along it. At 120 min, the leading edge of the steam chamber at the cap rock is about one-third of the lateral length of the model. During steam chamber expansion, steam in the lower part of the interlayer floats upward along the left side of the injection well, limiting steam chamber development in the lower part of the interlayer and resulting in a smaller expansion area. In the later stage (120–300 min), the steam chamber

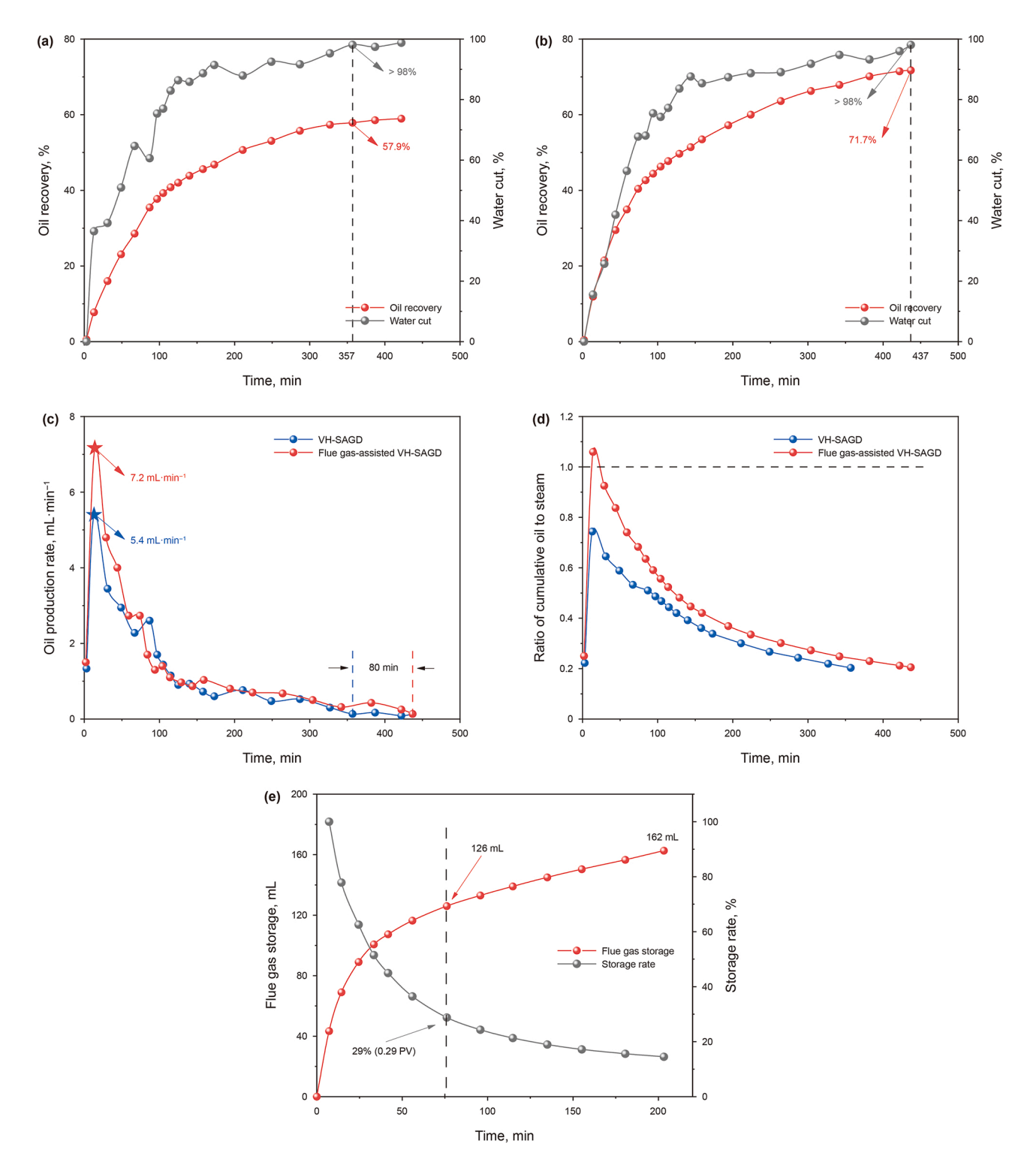


Fig. 8. Comparison of the oil displacement dynamics between VH-SAGD and flue gas-assisted VH-SAGD. (a) Oil recovery and water cut of VH-SAGD; (b) oil recovery and water cut of flue gas-assisted VH-SAGD; (c) oil production rate; (d) cumulative oil-steam ratio; (e) flue gas storage.

primarily develops longitudinally, but significant heat dissipation during upward steam movement causes the leading edge to advance in a sloped shape.

During the same period, the steam chamber expansion area and rate of flue gas-assisted VH-SAGD were both greater than those of VH-SAGD. As shown in Fig. 5, at 50 min, the upper edge of the steam chamber of the flue gas-assisted VH-SAGD has reached the cap rock. At 120 min, the leading edge of the steam chamber at the caprock is nearly half the lateral length of the model. The steam chamber expansion rates in both methods decrease over time, but the decline rate is significantly lower for flue gas-assisted VH-SAGD than for VH-SAGD (Fig. 6). After 300 min of oil displacement, the steam sweep efficiency of flue gas-assisted VH-SAGD is 32%, which is 12.47% higher than that of VH-SAGD. This means that about 38% of the steam can be saved by achieving the same wave volume.

The comparison of the oil sand distributions and typical oil displacement phenomena is shown in Fig. 7. During the VH-SAGD process, the rapid heat dissipation of steam to the reservoir rock matrix and the caprock results in the steam chamber developing mainly in the upper-left corner of the model, especially in lowpermeability reservoirs. However, the lateral expansion of the top steam chamber is limited, and the vertical gravity drainage effect directly above the horizontal production well is relatively weak. The thermal fluid primarily flows toward the production well in the manner depicted as pattern ① in Fig. 7(a). This occurs because, in regions distant from the production well, heavy oil flowing downward under gravity is driven laterally toward the production well through channels created by horizontal forces. The interlayer acts as the cap layer of the low-permeability reservoir at the bottom of the model, which inhibits the uplift of steam to the high-permeability layer and promotes the lateral flow of steam along the interlayer in the form of pattern ②. This effectively improves the lateral development of the steam chamber in the lower part of the model, similar to the mechanism of the hybrid steam drive/SAGD process and the hybrid CSS/SAGD process in enhancing oil recovery in reservoirs containing lean zones (Xu et al., 2014, 2017). Compared with SAGD, this method is more suitable for the development of heavy oil reservoirs with lean zones and thinner layers, but it needs optimize the location of the vertical well in combination with the distribution characteristics of the lean zones.

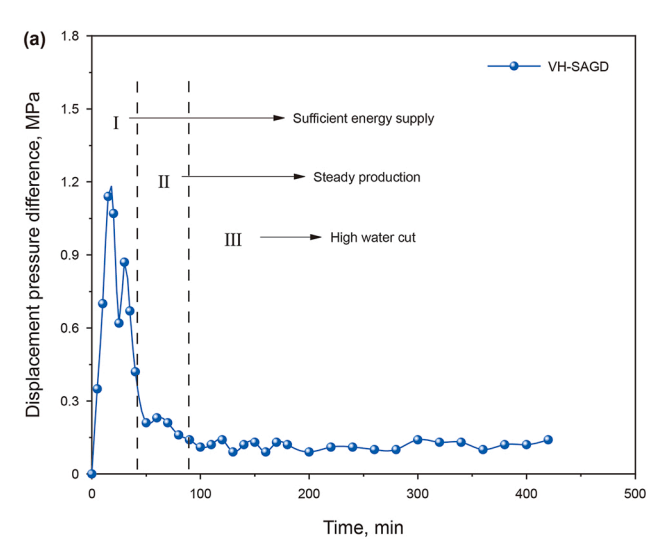
With the synergistic effect of the flue gas, the lateral migration

distance of steam and the gravity oil drainage efficiency are significantly improved. As shown in Fig. 7(b), the enhanced flow pattern ② results in the leading edge of the steam chamber in the low-permeability layer extending beyond the right end of the interlayer, with pattern 3 demonstrating a more significant drainage effect compared to VH-SAGD. It is analyzed that the mechanism of flue gas-induced lateral steam migration involves two key factors. (1) Creation of lateral flow channels: When the upward migration of flue gas beneath the interlayer is obstructed, its non-condensable and highly diffusive characteristics cause it to accumulate and form fingering effect, which establish lateral migration pathways for thermal fluids, including steam, as depicted in Fig. 7(c). (2) Reduction of flow resistance: The dissolution of flue gas lowers the threshold pressure of heavy oil, thereby reducing the resistance to lateral steam migration. There is another factor for the improvement in thermal sweep efficiency. The flue gas accumulated at the reservoir top not only minimizes steam heat loss but also compensates for energy deficits caused by channeling and other unidentified factors (Austin-Adigio and Gates, 2019), thereby driving the lateral oil displacement and vertical drainage in VH-SAGD (Fig. 7(d)).

#### 3.1.2. Oil displacement dynamics

To objectively characterize oil displacement in VH-SAGD and flue gas-assisted VH-SAGD, the produced liquid was placed in a high-temperature oven for 24 h to ensure complete oil-water separation. During settling, the containers were sealed with plastic wrap to prevent water evaporation.

Fig. 8 shows the oil displacement dynamics of VH-SAGD and flue gas-assisted VH-SAGD. The oil recovery of the two displacement modes rapidly increases at the beginning, followed by a gradual decline in the oil production rate at the middle to later stages. The recovery rate slowly increases and eventually stabilizes, with VH-SAGD achieving a final oil recovery of 58.9%. The limited thermal range of pure steam keeps the viscosity of heavy oil high in unheated regions, and the highly mobile condensed water tends to channel. This is especially noticeable in the later stages, where fluid channeling creates high-permeability paths, leading to substantial steam heat loss (Dong et al., 2019). Comparing Fig. 8(a) and (b), the final oil recovery of flue gas-assisted VH-SAGD is 71.7%, which is 12.8% higher than VH-SAGD. Analysis suggests that combining flue gas with steam increases the total flow rate of the displacing fluid, which significantly



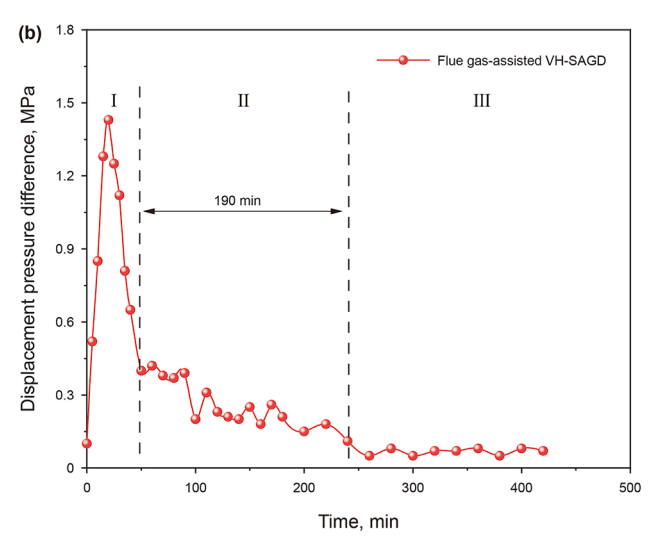


Fig. 9. Variation curve of the displacement pressure difference with time. (a) VH-SAGD; (b) flue gas-assisted VH-SAGD.

boosts the oil production rate during the piston-like displacement stage before gas channeling occurs. As shown in Fig. 8(c), the maximum oil production rate of flue gas-assisted VH-SAGD is 7.2 mL·min<sup>-1</sup>, which is 1.8 mL·min<sup>-1</sup> higher than that of VH-SAGD.

Moreover, the improvement in the oil recovery with the assistance of flue gas is reflected in the extended production time. The displacement end time for flue gas-assisted VH-SAGD is 437 min, 80 min longer than VH-SAGD. This occurs because after gas or water channeling, flue gas can convert the oil-water two-phase flow into an oil-gas-water three-phase flow in VH-SAGD. The bubbles formed by it and the oil and water phases will produce the Jamin effect (Wright, 1933) when they migrate in throats in the porous medium, forcing the flow channels to expand and sustaining crude oil production in a scraping manner.

As a byproduct of steam, flue gas offers not only short-term economic advantages over other additives but also long-term benefits in terms of environmental and reservoir sustainability for flue gas-assisted VH-SAGD. As shown in Fig. 8(d), at the end of the displacement, the cumulative oil-steam ratio of the two modes are approximately 0.2. but flue gas-assisted VH-SAGD operates 80 min longer than VH-SAGD. When the flue gas injection volume reaches 1 PV, nearly one-third of the flue gas remains in the reservoir in the form of free gas and dissolved gas (Fig. 8(e)), which is higher than that of flue gas-assisted steam flooding (Wang et al., 2022). The emphasis on the dual-phase capture (structural capture and solubility capture) of CO<sub>2</sub> in flue gas not only aligns with decarbonization goals but also ensures a stable long-term impact on the reservoir, without significant adverse effects. This is because N<sub>2</sub> is more stable in nature and has weaker interactions with heavy oil and rocks. Dissolved CO2 enhances the distillation efficiency of steam through extraction and by improving heat exchange between steam and heavy oil molecules (Li et al., 2023), while free CO<sub>2</sub> stabilizes asphaltenes through competitive adsorption (reducing aggregate size). These mechanisms collectively improve the longterm mobility of heavy oil. Although prolonged CO<sub>2</sub> exposure may induce rock mineral dissolution (Mikunda et al., 2021), the risk of formation damage from this reaction can be minimized by preinjecting low-salinity water (Othman et al., 2019).

Fig. 9 shows the variation in the displacement pressure difference over time. The entire displacement process can be divided into three stages: sufficient energy supply stage, steady production stage, and high-water cut stage. In the stage of sufficient energy supply, the maximum displacement pressure for VH-SAGD is 1.14 MPa, and after steam breakthrough, it quickly shifts to the high water cut stage, with a relatively short steady production stage. In contrast, the maximum displacement pressure difference for flue gas-assisted VH-SAGD is 1.43 MPa, 0.29 MPa higher than VH-SAGD, and the duration of steady production is significantly extended from less than 50–190 min. This indicates that the

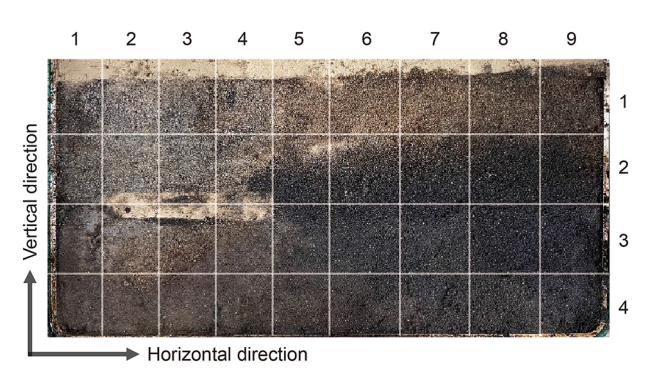
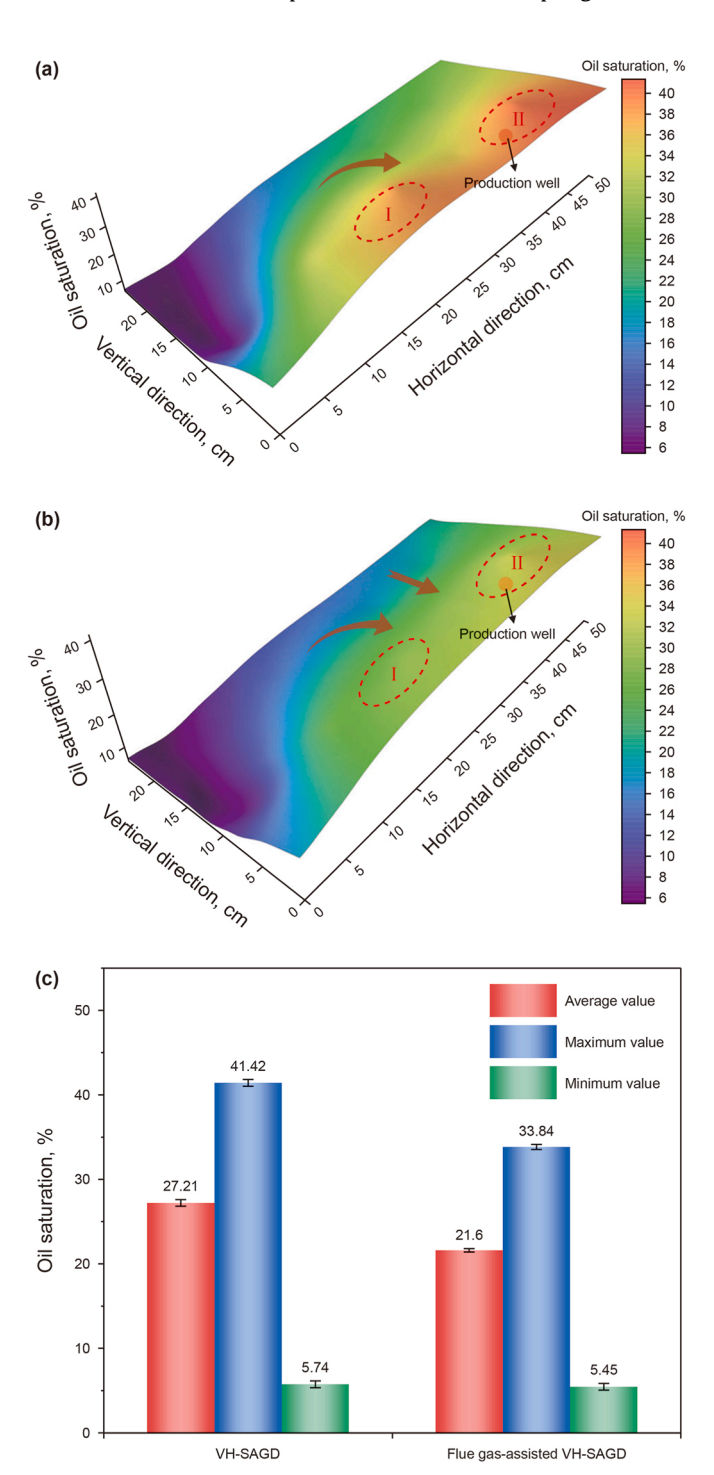


Fig. 10. Distribution of the oil sand.

expansion of the flue gas during the formation of high permeability channels can make up for the energy deficit of the reservoir to a certain extent. More importantly, the gas dissolved in heavy oil is gradually released, promoting foam oil generation, which helps alleviate the decline in oil recovery due to channeling and delays the onset of the high-water cut period.

# 3.1.3. Remaining oil distribution

After the oil displacement experiment, oil sand samples were collected from the 2D flat plate model. The 36 sampling locations



**Fig. 11.** Comparison of the oil saturation fields. (**a**) VH-SAGD; (**b**) flue gas-assisted VH-SAGD; (**c**) quantitative comparison.

are shown in Fig. 10. The samples at each location were divided into 3 parts, and the average value was calculated after the oil saturation was measured.

Fig. 11 shows the oil saturation fields of VH-SAGD and flue gasassisted VH-SAGD. In both cases, the mobilization of heavy oil in the high-permeability layer above the interlayer is relatively higher than in the low-permeability laver below the interlayer. The oil saturation near the injection well remains relatively low. In the VH-SAGD experiment, the areas with the highest oil saturation are I and II, at 40% and 38%, respectively. A significant decrease in oil saturation occurs between these two areas, to the left of the horizontal well, forming a distinct concave. This indicates that the thermal fluid does not effectively pass through low-permeability area I but migrates from the high-permeability layer downward to the production well, as shown by the red arrows in Fig. 11(a), providing further evidence for the discussion in Section 3.1.1. In flue gas-assisted VH-SAGD, the oil saturation in each region decreases compared to VH-SAGD, with an average saturation of 21.6%, which is 5.6% lower than that in VH-SAGD. The highest oil saturation is less than 34% (Fig. 11(c)). The utilization degree of heavy oil in the low-permeability layer below the interlayer has been improved, especially in areas I and II. This is due to the strong diffusion capacity of flue gas, which mobilizes residual oil that has not been significantly heated. Meanwhile, the oil saturation in the high-permeability layer at the top of the production well decreases, and the concavity between areas I and II becomes less pronounced (Fig. 11(b)). This indicates that under the action of flue gas, the heating degree of heavy oil in the high-permeability layer on the right side of the model increases, and the oil drainage area increases, which diversifies the flow path of thermal fluid and fully utilizes the characteristics of the VH-SAGD well type.

# 3.2. Effect of pre-injection gas on flue gas-assisted VH-SAGD

Although flue gas-assisted VH-SAGD has shown promising results, the relationship between the flue gas injection method and oil displacement effectiveness remains unknown. In the flue gas-assisted VH-SAGD experiment with pre-injection gas, 0.25 PV of flue gas was injected into the model before the co-injection of flue gas and steam.

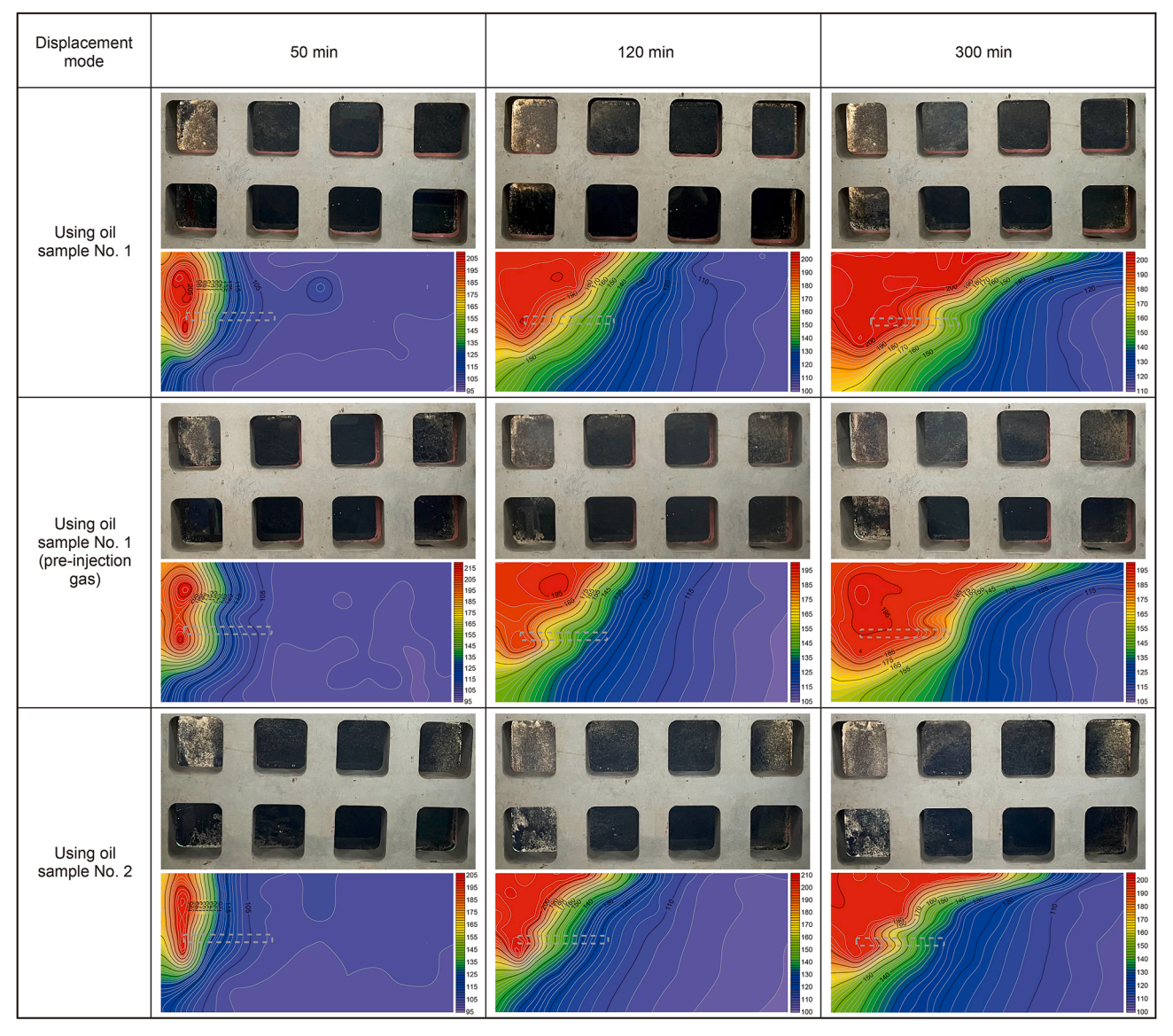


Fig. 12. Steam chamber expansion and temperature field changes for the three types of flue gas-assisted VH-SAGD.

#### 3.2.1. Steam chamber development

Fig. 12 shows the steam chamber expansion and temperature field changes for three types of flue gas-assisted VH-SAGD. Preinjection gas results in a faster steam chamber development speed during the early development stage (0-50 min). Both the high and low permeability layers exhibit a trend of lateral development. At the middle stage of development (50–120 min), the development rate of the low-permeability layer declines, while the development of the high permeability layer steam chamber is basically the same as that of the direct co-injection. At the later stage of development (120-300 min), the expansion trend of the steam chamber is characterized primarily by lateral expansion in the high-permeability layer and weak radiation in the lowpermeability layer. By the end, the lower part of the steam chamber develops over a greater distance compared to direct coinjection, but the development in the upper part of the steam chamber is slightly inferior.

As the viscosity of heavy oil increases, the area of the steam chamber decreases during each displacement stage. Because of the deterioration of heavy oil fluidity, it is more difficult to push the steam laterally, and the steam chamber mainly expands upward along the injection wells. After steam overlap, the trend of steam chamber expanding laterally along the caprock only applies to the top of the model, with weaker lateral development in the middle

and lower parts. At 120 min, the leading edge of the steam chamber at the caprock is slightly larger than one-third of the length of the model. By the end of the experiment, the steam chamber in the low-permeability lower layer of the interlayer remains weakly developed.

During the oil displacement, the expansion rate of the steam chamber was recorded, and after completion, the thickness of the steam overlap and the development length of the steam chamber in the middle and lower parts of the oil reservoir were measured. The results are shown in Fig. 13. The steam chamber in the flue gasassisted VH-SAGD conducted with simulated oil sample No. 2 occupies 20.4% of the entire model, a decrease of 11.6% compared to simulated oil sample No. 1. Additionally, the development distance of the steam chamber in the middle and lower parts of the oil reservoir and the development thickness of the steam chamber at the cap layer decrease by 3.5 and 3.0 cm, respectively. In the early stage, the steam chamber expansion rate with pre-injection gas is greater than with direct co-injection. By the end, the development distance of the steam chamber in the middle and lower parts of the oil reservoir increases by 6 cm compared to direct co-injection, and the steam chamber proportion increases by 1.5%. The key reason lies in the significant differences in the steam chamber development patterns between the two modes. The flue gas preinjected in the early stage is not heated, resulting in weaker

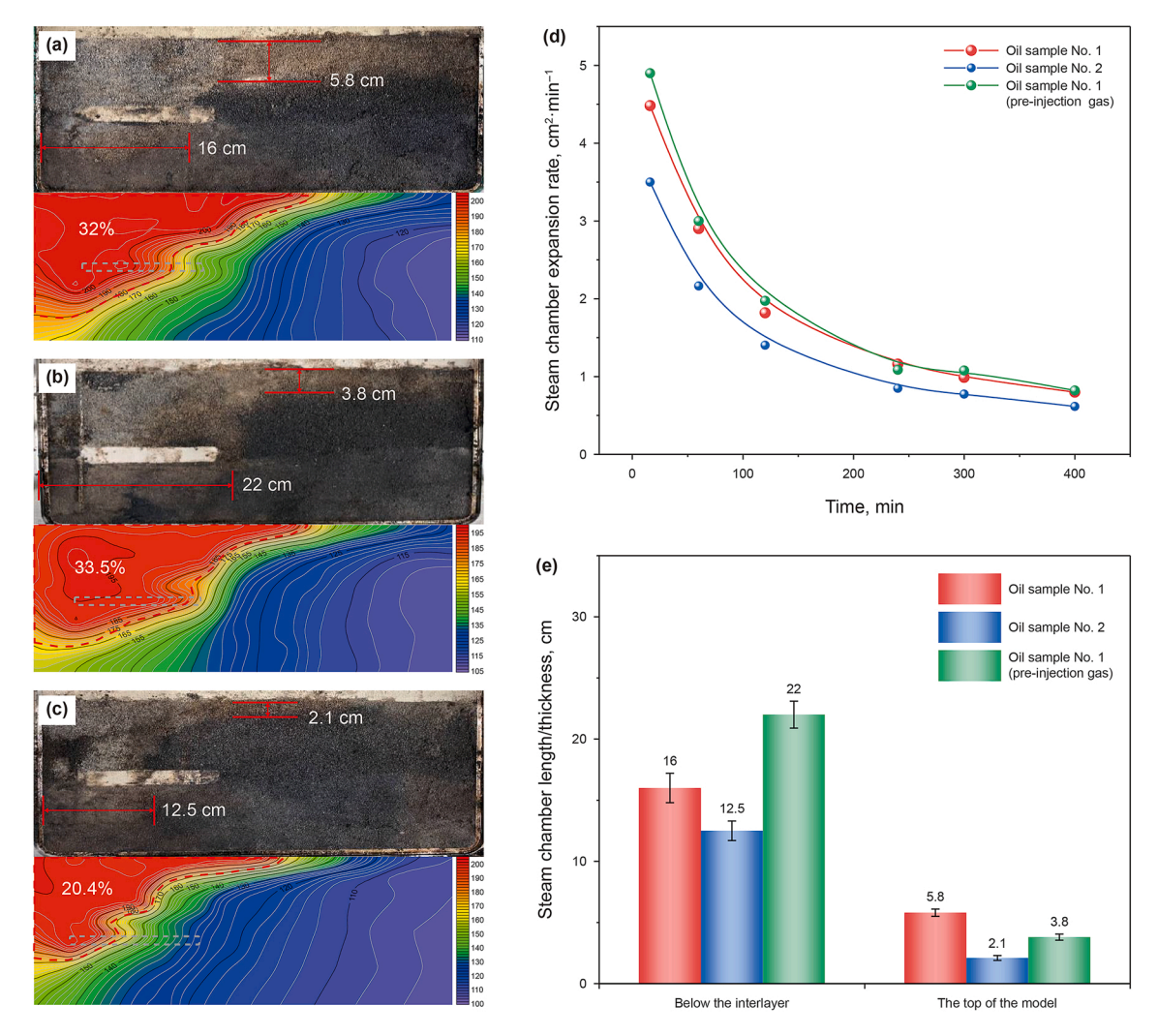


Fig. 13. Quantitative comparison of the oil sand distribution and steam chamber. (a) Flue gas-assisted VH-SAGD using oil sample No. 1; (b) flue gas-assisted VH-SAGD under preinjection gas; (c) flue gas-assisted VH-SAGD using oil sample No. 2; (d) comparison of steam chamber expansion rate; (e) quantitative comparison of the steam chambers.

upward dynamics. Its flow direction is horizontal (toward the outlet), and the resulting flow channels can directly induce lateral steam migration once co-injection begins. This increases the initial steam chamber expansion rate and extends the lateral development distance of the steam chamber in both the middle of the reservoir and the low-permeability layer.

#### 3.2.2. Oil displacement dynamics

Fig. 14 shows the oil recovery dynamics of the three types of flue gas-assisted VH-SAGD experiments. The oil recovery with preinjection gas is 73.8%, which is a slight improvement compared to direct co-injection. While the oil recovery and water cut for both injection methods increase rapidly at first and then gradually slow down before stabilizing, the variation in the slope of the oil recovery curve for pre-injection gas is relatively low. This difference can be attributed to the formation of microchannels within the reservoir under the influence of pre-injection gas, reducing the threshold pressure at the piston oil displacement stage. This accelerates the development of the steam chamber at the early stage of displacement. The advantage of the gas pre-injection in comparing oil production rate mode is more intuitive. While the maximum oil production rate decreases from 7.2 to 6.7 mL·min<sup>-1</sup>, the oil production rate during the steady production phase with pre-injection

gas is clearly higher than with direct co-injection, becoming similar only at 200 min (Fig. 14(b)). This explains how the higher oil recovery is achieved despite the lower maximum oil production rate.

The results discussed above are further supported by the comparison of pressure difference changes (Fig. 14(d)). With preinjection gas, the maximum displacement pressure difference is 1.18 MPa, which is slightly lower than with direct co-injection. However, the pressure drop after the peak is relatively small. Moreover, the pressure peak in flue gas-assisted VH-SAGD occurs later than that in gas pre-injection. This is because the permeation channels established by pre-injection gas create a larger affected area for subsequent oil displacement, requiring more fluid injection to replenish energy.

An excessive viscosity of heavy oil exerts a negative impact on oil recovery. The oil recovery for simulated oil sample No. 1 is 71.7%, which is 7.6% lower than that for simulated oil sample No. 2. The maximum oil production rate is 6.9 mL·min<sup>-1</sup>, which is not significantly different from the simulated oil sample No. 1, with only a decrease of 0.3 mL·min<sup>-1</sup>. Notably, when using simulated oil sample No. 2, the water cut reaches 80% in 97 min, which is 32 min earlier than with simulated oil sample No. 1. This indicates that the early arrival of the high-water cut period is a significant factor contributing to the reduction in oil recovery for highly viscous

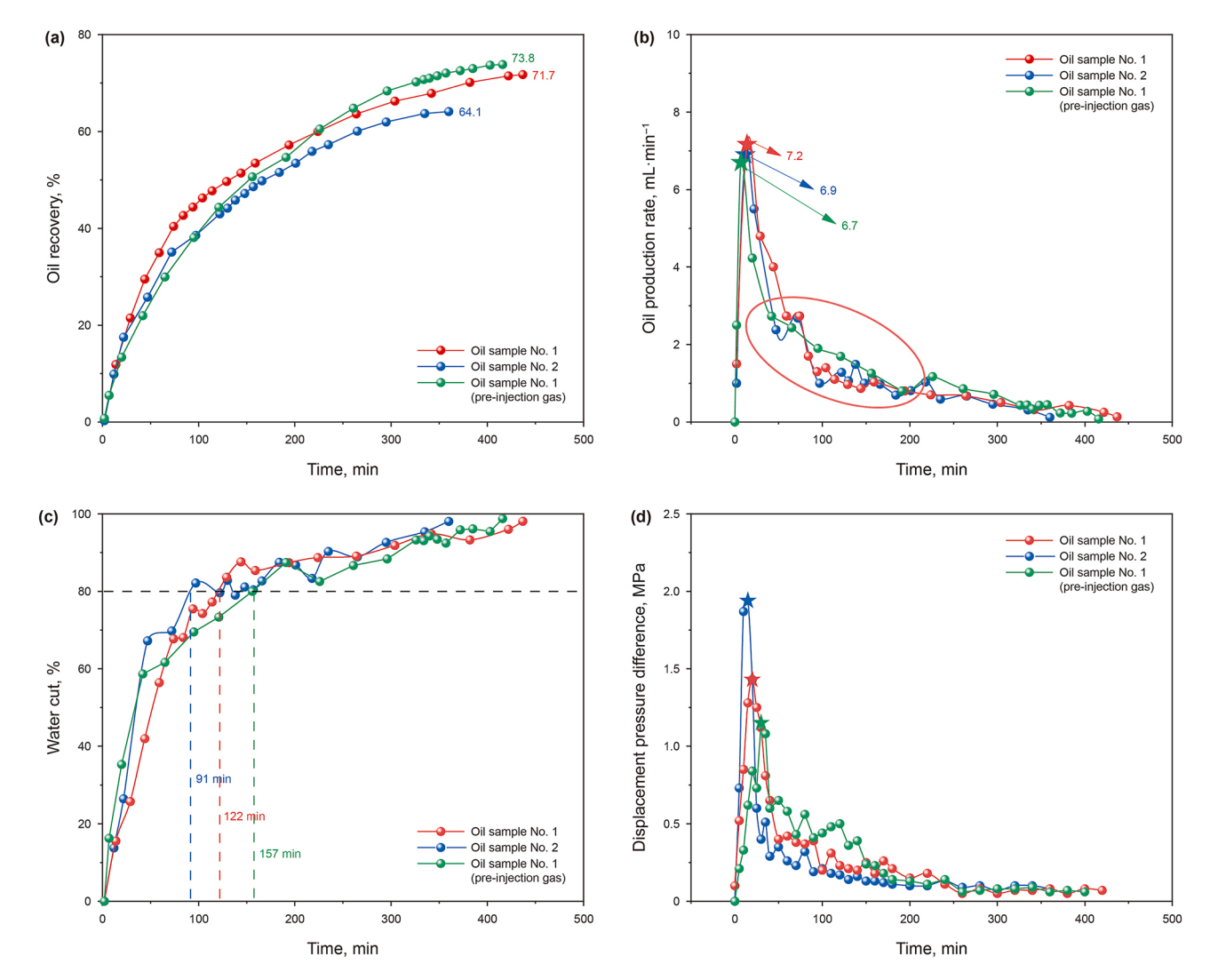


Fig. 14. Comparison of the oil displacement dynamics for the three types of flue gas-assisted VH-SAGD experiments. (a) Oil recovery; (b) oil production rate; (c) water cut; (d) displacement pressure difference.

heavy oil.

#### 3.2.3. Remaining oil distribution

Fig. 15 shows the 3D distribution of the oil saturation for the three types of flue gas-assisted VH-SAGD experiments. The most obvious characteristic of pre-injection gas is that the oil saturation in the low-permeability layer below the interlayer is significantly lower than in direct co-injection. This also corresponds well to the development characteristics of the steam chamber for both injection modes, indicating that this approach improves the steam flow environment and enhances the heating of the low-permeability layer. In the experiment conducted using simulated oil sample No. 2, the oil saturation in various regions of the model is higher than that in the experiment conducted with simulated oil sample No. 1, and this difference is larger in the low-permeability layer below the interlayer and on the right side of the top of the model. The largest difference is observed in the lower-right corner, where the oil saturation for simulated oil sample No. 2 is close to 38%, while that for simulated oil sample No. 1 is only 35%. Therefore, when applying flue gas-assisted VH-SAGD, pre-injection flue gas before flue gasassisted VH-SAGD can positively impact the expansion of the steam chamber, provided the gas injection volume is wellcontrolled. The viscosity of the heavy oil should not be too high; otherwise, the system may prematurely enter a high-water-cut phase, disrupting the synergy between oil displacement and oil drainage.

# 3.3. Effect of interlayer length on flue gas-assisted VH-SAGD

The fluid flow and the final development of the steam chamber are closely related to the characteristics of the position of the barrier layer (Kumar and Hassanzadeh, 2021). To clarify the impact of interlayer length on fluid migration characteristics during oil displacement and to optimize well placement strategies in actual field operations, further experiments were conducted on flue gasassisted VH-SAGD with different interlayer lengths (0, 15, 25, 35 cm) based on the methods described in Section 2.4.

Fig. 16 shows the oil recovery of flue gas-assisted VH-SAGD with different interlayer lengths. The oil recovery first increases and then decreases as the ratio of the interlayer length to the well spacing increases. The oil recovery peaks at 72.6% when the ratio is 0.5. As the ratio increases to 0.7, the recovery decreases to 69.4%, which is lower than the recovery of 69.8% without interlayer. It is important to note that when the ratio of interlayer length to well spacing is less than 0.5, the oil recovery increases at a gradually rising pace. These characteristics suggest that when there is no interlayer or the interlayer length is very short, its impact on recovery efficiency is minimal. When the length of the interlayer is about half of the well spacing, it is more conducive to improving the development efficiency.

Fig. 17 shows the schematic of steam chamber development mechanism under the influence of the interlayer. A relatively small interlayer length exerts a weak impact on the upward movement of steam and downward flow of hot water. Because the lateral development distance of the steam chamber at the early stage of

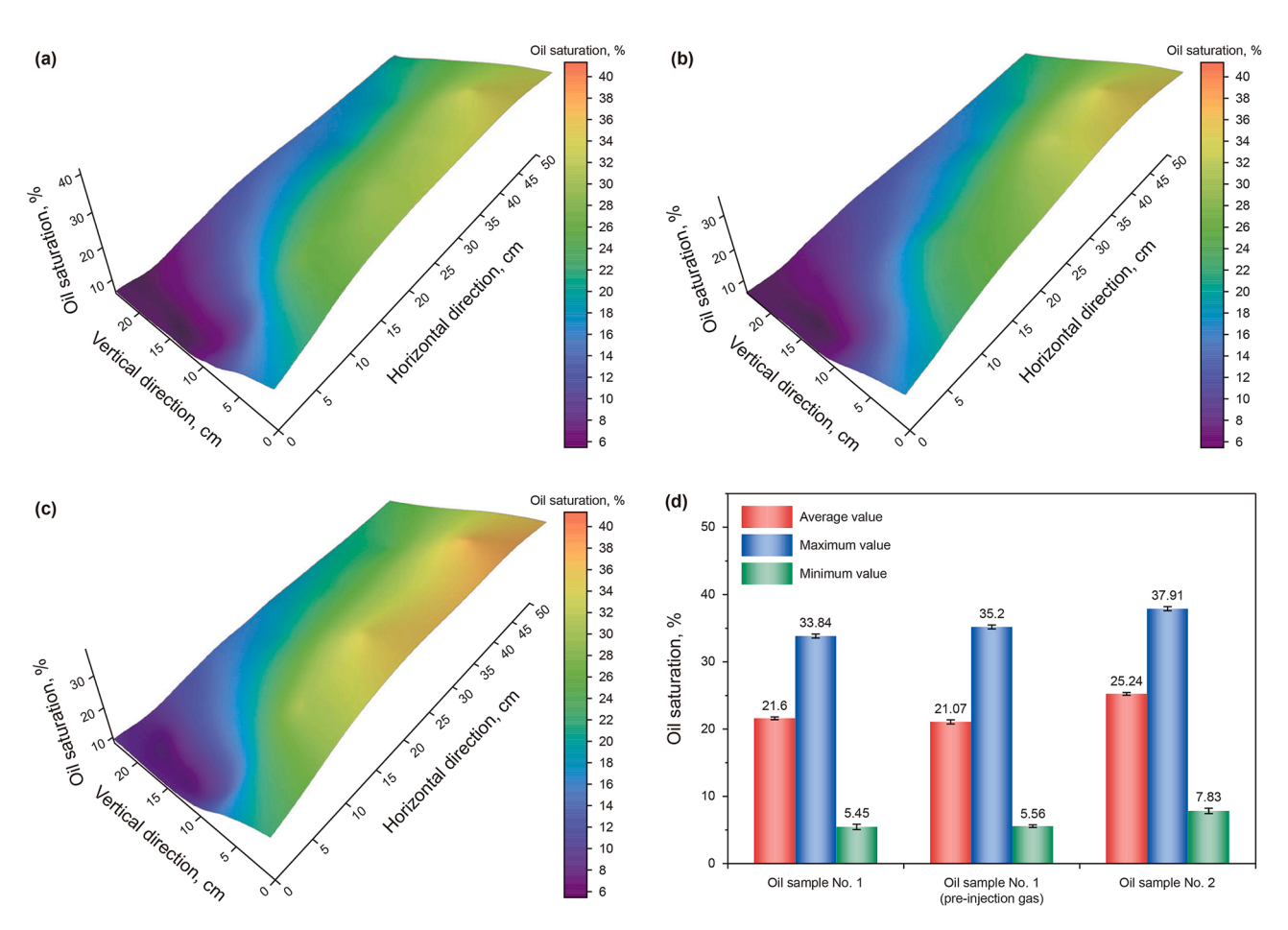


Fig. 15. Comparison of the oil saturation fields. (a) Flue gas-assisted VH-SAGD using oil sample No. 1; (b) flue gas-assisted VH-SAGD under gas pre-injection; (c) flue gas-assisted VH-SAGD using oil sample No. 2; (d) quantitative comparison.

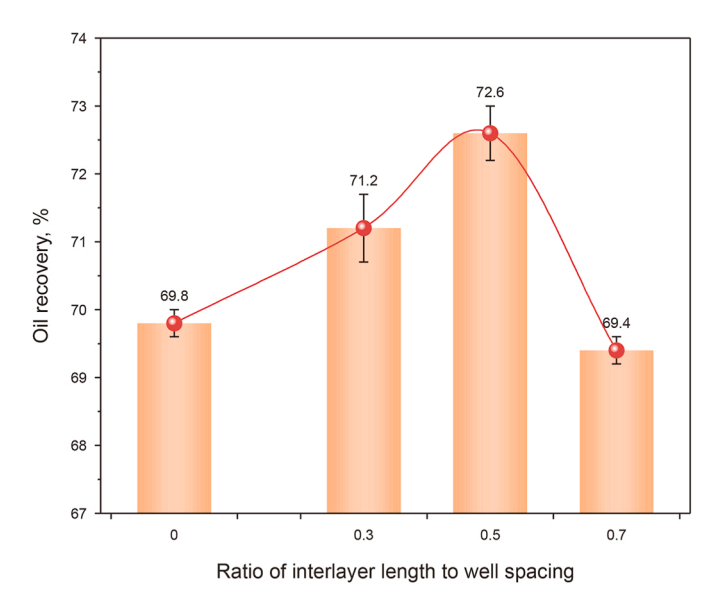


Fig. 16. Effect of interlayer length on the oil recovery of flue gas-assisted VH-SAGD.

development can easily exceed the interlayer length. Although this may affect the fluid streamlines inside the steam chamber, it is essentially similar to steam flooding with dual vertical wells, as shown in Fig. 17(a). When the interlayer length is too long, the downward movement of the condensed hot water from the high-permeability layer above the interlayer is obstructed. As a result, the hot water flows laterally along the top of the interlayer but struggles to bypass it. Similarly, the lateral development of the steam chamber in the low-permeability layer beneath the interlayer is limited, as shown in Fig. 17(c). Although steam gradually accumulates beneath the interlayer, the spatial position is not conducive to oil drainage. As a result, most of the steam flows to the production well in the form of channeling, making the oil in the low-permeability layer even more difficult to recover.

For heavy oil reservoirs with confirmed interlayers, it is essential to select appropriate injection-production well locations based on the injection-production parameters of steam and flue gas. The spacing between vertical and horizontal wells should ideally be maintained at about twice the length of the interlayer. Because this is more conducive to promoting the lateral expansion of the lower steam chamber in the model. As shown in Fig. 17(b), The steam injected from the low-permeability layer gradually rises and bypasses the interlayer, flowing upward along the right side of the interlayer. Simultaneously, condensed hot water from the

high-permeability layer flows downward along the displacement front. Under the convective action of rising steam and downward-flowing condensed water, the lateral development of the steam chamber in the middle and lower parts of the reservoir is significantly improved. This phenomenon has been partially confirmed through numerical simulations and industrial-scale experiments (Wang et al. 2020, 2023a; Zhang et al., 2022). For example, the Xinjiang Oilfield in China has adopted a vertical and horizontal well spacing of 15–35 m based on the width of the interlayer, which has increased the oil to gas ratio from 0.13 to 0.14, effectively alleviating the negative impact of the interlayer. However, this optimization is based on pure steam. With the combined effects of flue gas and steam, the actual development performance of reservoirs with interlayers is anticipated to improve further.

#### 4. Conclusions

In this work, a series of 2D visualization experiments were conducted focusing on flue gas-assisted VH-SAGD. The combined effects of flue gas and VH-SAGD in a heterogeneous environment were explored, and the interlayer length was optimized to enhance oil recovery. The obtained results are as follows:

- (1) Compared to that of VH-SAGD, the oil recovery of flue gasassisted VH-SAGD increases from 58.9% to 71.7%, better leveraging the well-type characteristics of VH-SAGD. From the perspective of thermal sweep efficiency, maintaining the same sweep volume, the steam injection volume can be reduced by approximately 38%. The flue gas can significantly increase the thickness of steam accumulation at the top of the reservoir. Additionally, by supplementing the energy of the steam chamber, the oil drainage area of VH-SAGD is further expanded.
- (2) The flow channels formed by pre-injection gas can induce lateral steam migration, slow down steam rise, and the gas dissolution process can reduce crude oil viscosity in advance, improving the steam flow environment and increasing the lateral development distance of the steam chamber in the low-permeability layer. When the injection volume is controlled at 0.25 PV, pre-injecting flue gas increases the oil recovery of flue gas-assisted VH-SAGD by 2.1%
- (3) For flue gas-assisted VH-SAGD, the distance between the vertical and horizontal wells is twice that of the interlayer, which is more beneficial in transforming the negative effects of the interlayer into advantages. When the lateral development distance of the steam chamber in the lowpermeability layer is just beyond the interlayer, upward

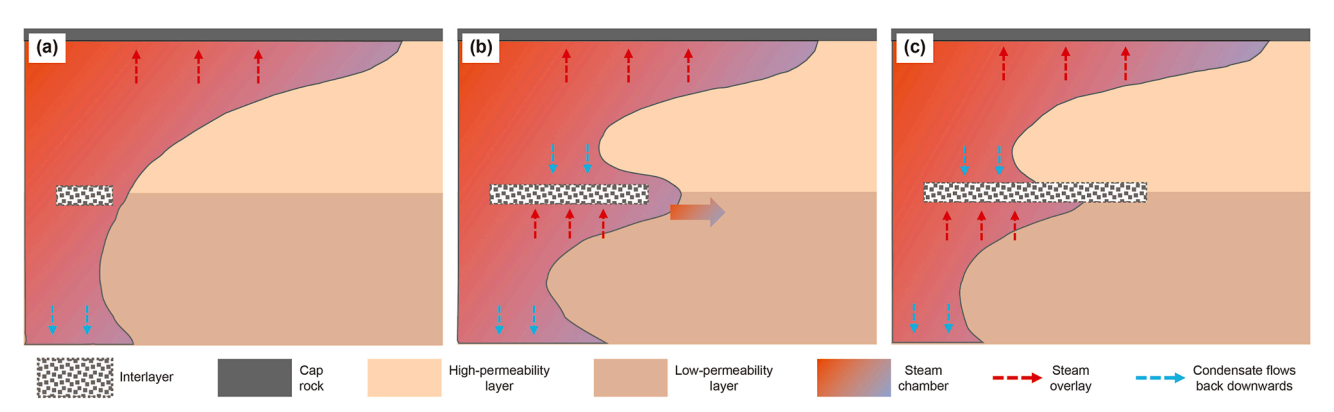


Fig. 17. Schematic of steam chamber development mechanism under the influence of the interlayer.

and downward convection of floating steam and reflux condensate will enhance heating in the lower part of the reservoir, which can better leverage the oil displacement advantage of the vertical well without affecting the oil drainage effect.

#### **CRediT authorship contribution statement**

**Bin-Fei Li:** Writing – review & editing, Validation, Supervision, Resources, Project administration, Methodology, Conceptualization. **Bo-Liang Li:** Writing – original draft, Investigation, Formal analysis, Data curation, Conceptualization. **Xin-Ge Sun:** Methodology, Investigation. **Di Zhu:** Methodology, Investigation. **Sen Chen:** Investigation, Data curation. **Zhao-Min Li:** Funding acquisition. **Lei Tao:** Validation, Investigation. **Jun-Hao Zhang:** Investigation.

# Data availability

Data will be made available on request.

# **Declaration of competing interest**

The authors declare that they have no known competing financial interests or personal relationships that could have appeared to influence the work reported in this paper.

# Acknowledgments

Financial support for this work is received from the National Natural Science Foundation of China (Grant No. U22B20144). We also acknowledge the Shandong Engineering Research Center of Carbon Dioxide Utilization and Storage for their support and assistance in this experimental research.

#### References

- Al-Bahlani, A.M., Babadagli, T., 2009. SAGD laboratory experimental and numerical simulation studies: a review of current status and future issues. J. Pet. Sci. Eng. 68 (3–4), 135–150. https://doi.org/10.1016/j.petrol.2009.06.011.
- Alomair, O.A., Alajmi, A.F., 2022. A novel experimental nanofluid-assisted steam flooding (NASF) approach for enhanced heavy oil recovery. Fuel 313, 122691. https://doi.org/10.1016/i.fuel.2021.122691.
- Austin-Adigio, M., Gates, I., 2019. Non-condensable gas co-injection with steam for oil sands recovery. Energy 179, 736–746. https://doi.org/10.1016/j.energy.2019.05.034.
- Bai, Y.F., 2015. Research on Technology of Steam Flooding and Gravity Drainage Development in Super Heavy Oil Reservoir of Chunhui Oilfield. Master Thesis. China University of Petroleum (East China) (in Chinese).
- Bata, T., Schamel, S., Fustic, M., Ibatulin, R., 2019. AAPG Energy Minerals Division Bitumen and Heavy Oil Committee Annual Commodity Report—May 2019. American Association of Petroleum Geologists (AAPG).
- Butler, R.M., Mcnab, G.S., Lo, H.Y., 1981. Theoretical studies on the gravity drainage of heavy oil during in-situ steam heating. Can. J. Chem. Eng. 59 (4), 455–460. https://doi.org/10.1002/cjce.5450590407.
- Chen, H., Wang, Z., Wang, K., Li, Z., Li, S., 2020. Investigation of EOR mechanism for flue gas assisted SAGD. J. Pet. Sci. Eng. 193, 107420. https://doi.org/10.1016/j.petrol.2020.107420.
- Cui, G., Liu, T., Xie, J., Rong, G., Yang, L., 2022. A review of SAGD technology development and its possible application potential on thin-layer super-heavy oil reservoirs. Geosci. Front. 13 (4), 101382 https://doi.org/10.10.1016/j. gsf.2022.101382.
- Dong, X., Liu, H., Chen, Z., Wu, K., Lu, N., Zhang, Q., 2019. Enhanced oil recovery techniques for heavy oil and oilsands reservoirs after steam injection. Appl. Energy 239, 1190–1211. https://doi.org/10.1016/j.apenergy.2019.01.244.
- Gao, Y., Liu, S., Shen, D., Guo, E., Bao, Y., 2008. Improving oil recovery by adding N<sub>2</sub> in SAGD process for super-heavy crude reservoir with top-water. In: SPE Russian Petroleum Technology Conference. https://doi.org/10.2118/114590-MS.
- Gao, Y., Ren, Z., Chen, M., 2022. Coupled geomechanical-thermal simulation for oil sand reservoirs with shale barriers under hot water injection in vertical wellassisted SAGD wells. J. Pet. Sci. Eng. 208, 109644. https://doi.org/10.1016/j.

petrol.2021.109644.

- Guo, K., Li, H., Yu, Z., 2016. In-situ heavy and extra-heavy oil recovery: a review. Fuel 185, 886–902. https://doi.org/10.1016/j.fuel.2016.08.047.
- Hocking, G., Cavender, T.W., Person, J., 2011. Single-well SAGD: overcoming permeable lean zones and barriers. In: SPE Canada Unconventional Resources Conference. https://doi.org/10.2118/148832-MS.
- Huang, J., Zhang, J., Wang, L., 2015. Review of vapor condensation heat and mass transfer in the presence of non-condensable gas. Appl. Therm. Eng. 89, 469–484. https://doi.org/10.1016/j.applthermaleng.2015.06.040.
   Huang, S.J., Xiong, H., Wei, S.L., Huang, C.H., Yang, Y., 2016. Physical simulation of
- Huang, S.J., Xiong, H., Wei, S.L., Huang, C.H., Yang, Y., 2016. Physical simulation of the interlayer effect on SAGD production in mackay river oil sands. Fuel 183, 373–385. https://doi.org/10.1016/j.fuel.2016.06.104.
- Huang, S.J., Yang, L.J., Xia, Y., Du, M.G., Yang, Y.W., 2019. An experimental and numerical study of a steam chamber and production characteristics of SAGD considering multiple barrier layers. J. Pet. Sci. Eng. 180, 716–726. https://doi. org/10.1016/i.petrol.2019.05.062.
- Jamshid-nezhad, M., 2022. Steam alternating non-condensable gas injection for more heavy oil recovery. Energy 240, 122476. https://doi.org/10.1016/j. energy.2021.122476.
- Kumar, A., Hassanzadeh, H., 2021. Impact of shale barriers on performance of SAGD and ES-SAGD—a review. Fuel 289, 119850. https://doi.org/10.1016/j. fuel.2020.119850.
- Li, B., Li, B., Zang, Y., Zhu, D., Li, Z., Ruan, L., 2023. Experimental study of the distillation mechanism during coinjection of flue gas and steam for heavy oil development. Sep. Purif. Technol. 324, 124553. https://doi.org/10.1016/j. sepnur.2023.124553
- Li, Y., Wang, Z., Hu, Z., Xu, B., Zhao, J., 2020. A review of in situ upgrading technology for heavy crude oil. Petroleum 7 (5), 117–122. https://doi.org/10.1016/j.petlm.2020.09.004.
- Li, Y., Huang, D., Dong, X., Yang, D., 2024. Phase behaviour and physical properties of dimethyl ether (DME)/flue gas/water/heavy oil systems under reservoir conditions. Fuel 35, 129484. https://doi.org/10.1016/j.fuel.2023.129484.
- Liu, H., Cheng, L., Huang, S., Jia, P., Chen, M., 2018. Evolution characteristics of SAGD steam chamber and its impacts on heavy oil production and heat consumption. Int. J. Heat Mass Tran. 121, 579–596. https://doi.org/10.1016/j.ijheatmasstransfer.2018.01.038.
- Liu, Y., Xi, C., Liu, S., Liu, C., 2012. Impact of non-condensable gas on SAGD performance. In: SPE Heavy Oil Conference. https://doi.org/10.2118/150539-MS.
- Lu, N., Dong, X., Liu, H., Chen, Z., Xu, W., Zeng, D., 2024a. Molecular insights into the synergistic mechanisms of hybrid CO<sub>2</sub>-surfactant thermal systems at heavy oil-water interfaces. Energy 286, 129476. https://doi.org/10.1016/j. energy.2023.129476.
- Lu, T., Li, Z., Du, L., 2024b. Silica aerogel nanoparticle-stabilized flue gas foams for simultaneous CO<sub>2</sub> sequestration and enhanced heavy oil recovery. J. Clean. Prod. 434, 140055. https://doi.org/10.1016/j.jclepro.2023.140055.
- Mai, A., Bryan, J., Goodarzi, N., Kantzas, A., 2009. Insights into non-thermal recovery of heavy oil. J. Can. Pet. Technol. 48 (3), 27–35. https://doi.org/10.2118/
- Mikunda, T., Brunner, L., Skylogianni, E., Monteiro, J., Rycroft, L., Kemper, J., 2021. Carbon capture and storage and the sustainable development goals. Int. J. Greenh. Gas Control 108, 103318. https://doi.org/10.1016/j.ijggc.2021.103318.
- Nasr, T.N., Ayodele, O.R., 2006. New hybrid steam-solvent processes for the recovery of heavy oil and bitumen. In: Abu Dhabi International Petroleum Exhibition and Conference. https://doi.org/10.2118/101717-MS.
- Nguyen, H.X., Wisup, B., Tran, X., Ta, D.Q., Nguyen, H.D., 2012. Effects of reservoir parameters and operational design on the prediction of SAGD performance in Athabasca Oilsands. In: SPE Europec/EAGE Annual Conference. https://doi.org/ 10.2118/154778-MS.
- Othman, F., Naufaliansyah, M.A., Hussain, F., 2019. Effect of water salinity on permeability alteration during CO<sub>2</sub> sequestration. Adv. Water Resour. 127, 237–251. https://doi.org/10.1016/j.advwatres.2019.03.018.
- Pang, Z., Wang, L., Yin, F., Lyu, X., 2021. Steam chamber expanding processes and bottom water invading characteristics during steam flooding in heavy oil reservoirs. Energy 234, 121214. https://doi.org/10.1016/j.energy.2021.121214.
- Pierre, C., Barre, L., Pina, A., Moan, M., 2004. Composition and heavy oil rheology. Oil Gas Sci. Technol. 59 (5), 489–501. https://doi.org/10.2516/ogst:2004034.
- Santos, R.G., Loh, W., Bannwart, A.C., Trevisan, O.V., 2014. An overview of heavy oil properties and its recovery and transportation methods. Braz. J. Chem. Eng. 31 (3), 571–590. https://doi.org/10.1590/0104-6632.20140313s00001853.
- Sasaki, K., Akibayashi, S., Yazawa, N., Doan, Q.T., Ali, S.M.F., 2001. Experimental modeling of the SAGD process-enhancing SAGD performance with periodic stimulation of the horizontal producer. SPE J. 6 (1), 89–97. https://doi.org/ 10.2118/69742-PA.
- Speight, J.G., 2013. Heavy and Extra-heavy Oil Upgrading Technologies. Gulf Professional Publishing.
- Tamer, M., Gates, I.D., 2012. Impact of different SAGD well configurations (Dover SAGD phase B case study). J. Can. Pet. Technol. 51 (1), 32–45. https://doi.org/10.2118/155502-PA.
- Tao, L., Xu, L.L., Yuan, X., Shi, W.Y., Zhang, N., Li, S.Y., Si, Y., Ding, Y., Bai, J., Zhu, Q., Du, H., 2021. Visualization experimental study on well spacing optimization of SAGD with a combination of vertical and horizontal wells. ACS Omega 6 (44), 30050–30060. https://doi.org/10.1021/acsomega.1c04737.
- Wang, Q., Gao, X., Luo, C., Meng, X., Gan, S., Liu, J., 2020. Interlayer development patterns and SAGD enhanced oil recovery technology in the super heavy oil category-III reservoir. Special Oil Gas Reservoirs 27 (4), 105. https://doi.org/

- 10.3969/j.issn.1006-6535.2020.04.016 (in Chinese).
- Wang, Q., He, W., Gao, L., Gao, Y., 2023a. SAGD enhanced oil recovery technology of vertical well assisted double horizontal well in super heavy oil category-III reservoir. In: International Field Exploration and Development Conference. https://link.springer.com/chapter/10.1007/978-981-97-0264-0\_93.
- Wang, O., Yang, H., Liu, J., Gao, Y., Gao, L., 2023b. Optimization of SAGD key parameters for vertical assisted double horizontal wells in super heavy oil reservoir. J. Southwest Pet. Univ. (Sci. Technol. Ed) 45 (5), 81–87. https://doi. org/10.11885/j.issn.1674-5086.2021.06.21.01 (in Chinese).
- Wang, Z., Li, Z., Lu, T., Yuan, Q., Yang, J., Wang, H., Wang, S., 2017. Research on enhancing heavy oil recovery mechanism of flue gas assisted steam flooding. In: Carbon Management Technology Conference. https://doi.org/10.7122/
- Wang, Z., Li, S., Li, Z., 2022. A novel strategy to reduce carbon emissions of heavy oil thermal recovery: condensation heat transfer performance of flue gas-assisted steam flooding. Appl. Therm. Eng. 205, 118076. https://doi.org/10.1016/j. applthermaleng,2022,118076.
- Wei, S., Duan, Y., Wei, M., Ren, K., Lu, C., Zhan, J., Tang, Y., 2022. Experimental study on the effect of different distributed interlayer on SAGD performance. J. Pet. Sci. Eng. 209, 109827. https://doi.org/10.1016/j.petrol.2021.109827.
- Wright, R., 1933. Jamin effect in oil production. AAPG (Am. Assoc. Pet. Geol.) Bull. 17 (12) 1521-1526
- Xi, C., Qi, Z., Zhang, Y., Liu, T., Shen, D., Mu, H., Dong, H., Li, X., Jiang, Y., Wang, H., 2019.  $CO_2$  assisted steam flooding in late steam flooding in heavy oil reservoirs. Petrol. Explor. Dev. 46 (6), 1242–4250. https://doi.org/10.1016/S1876-3804(19)

- 60277-6.
- Xu, J., Chen, Z., Yu, Y., Cao, J., 2014. Numerical thermal simulation and optimization of hybrid CSS/SAGD process in Long Lake with lean zones. In: SPE Heavy Oil Conference. https://doi.org/10.2118/170149-MS.
- Xu, J., Chen, Z., Dong, X., Zhou, W., 2017. Effects of lean zones on steam-assisted gravity drainage performance. Energies 10 (4), 471. https://doi.org/10.3390/
- Zhang, X., Ma, M., Niu, L., Pang, C., Guan, X., 2014. Determination of oil content in oil sands. J. Zhengzhou Univ. (Sci. Ed.) 46 (3), 76–79. https://doi.org/10.3969/j. issn/1671-6841.2014.03.01 (in Chinese).
- Zhang, X., Zhou, Y., Du, X., Liu, P., 2022. Simulation and production optimization on enhanced oil recovery during the middle and late period for SAGD development in ultraheavy oil reservoirs with interlayers. Geofluids (1), 3474741. https://doi.org/10.1155/2022/3474741, 2022.
- Zhang, Y., Maini, B., 2020. Injection of non-condensable gas in SAGD using modified well configurations—a simulation study. In: Wu, Y., Carroll, J.J., Hao, M., Zhu, W. (Eds.), Gas Injection into Geological Formations and Related Topics. Wiley. https://doi.org/10.1002/9781119593324.ch17.
- Zhao, C., Sun, X., Lu, Y., Wang, L., Hu, P., Xing, X., Wang, G., 2023. Physical simulation experiment of steam chamber evolution in compound development of thin-layer ultra-heavy oil flooding and drainage. Lithol. Reserv. 35 (5), 161-168. https://doi.org/10.12108/yxyqc.20230516 (in Chinese).
  Zhao, D.W., Wang, J., Gates, I.D., 2014. Thermal recovery strategies for thin heavy
- oil reservoirs. Fuel 117, 431-441. https://doi.org/10.1016/j.fuel.2013.09.023.